Response of the mantle to flat slab evolution: Insights from local *S* splitting beneath Peru

Caroline M. Eakin[1], Maureen D. Long[1], Susan L. Beck[2], Lara S. Wagner[3], Hernando Tavera[4], and Cristóbal Condori[4]

[1]Department of Geology and Geophysics, Yale University, New Haven, Connecticut, USA, [2]Department of Geosciences, University of Arizona, Tucson, Arizona, USA, [3]Department of Geological Sciences, University of North Carolina at Chapel Hill, Chapel Hill, North Carolina, USA, [4]Instituto Geofísico del Perú, Lima, Peru

Abstract The dynamics of flat subduction, particularly the interaction between a flat slab and the overriding plate, are poorly understood. Here we study the (seismically) anisotropic properties and deformational regime of the mantle directly above the Peruvian flat slab. We analyze shear wave splitting from 370 local *S* events at 49 stations across southern Peru. We find that the mantle above the flat slab appears to be anisotropic, with modest average delay times (~0.28 s) that are consistent with ~4% anisotropy in a ~30 km thick mantle layer. The most likely mechanism is the lattice-preferred orientation of olivine, which suggests that the observed splitting pattern preserves information about the mantle deformation. We observe a pronounced change in anisotropy along strike, with predominately trench-parallel fast directions in the north and more variable orientations in the south, which we attribute to the ongoing migration of the Nazca Ridge through the flat slab system.

1. Introduction

Episodes of flat (or shallow) subduction have often been invoked to explain unusual geological observations that do not conform to the predictions of the standard plate tectonic model. For example, large-scale flat slab subduction of the Farallon plate during the Laramide orogeny has long been proposed as an explanation for widespread continental deformation [*Dickinson and Snyder*, 1978; *Bird*, 1988], the inboard migration of magmatism [*Coney and Reynolds*, 1977], and for stimulating ongoing small-scale convection beneath the western U.S. [*Humphreys*, 2009]. For South America, it has been suggested that during the Cenozoic most of the western margin has experienced alternating periods of flat and steep subduction, based upon a punctuated record of volcanism and tectonic evolution [e.g., *Ramos and Folguera*, 2009].

In order to understand better how plate tectonics has operated and evolved on our planet through geologic time, we need to be able to accurately recognize the expression of low-angle subduction in the geologic record. To do this we need to document the characteristics and properties of flat slabs that exist today, as well as try to understand the processes that form and maintain them. Many important questions relating to the dynamics and evolution of flat slabs still remain to be fully elucidated. For example, to what extent do flat slabs couple to the overriding plate? Is basal shear stress transferred to the surface? How does the mantle wedge deform? Does hydration generate a rheological weak zone between the flat slab and the continental crust? Or is the mantle relatively dry, strong, and more easily able to transmit stresses?

Deformation processes in the Earth's mantle, both past and present, are often best illuminated via observations of seismic anisotropy [e.g., *Long and Becker*, 2010]. In the upper mantle, seismic anisotropy is typically thought to result from the lattice-preferred orientation (LPO) of anisotropic minerals, such as olivine [e.g., *Karato et al.*, 2008] or serpentine [*Katayama et al.*, 2009; *Jung*, 2011]. Within a subduction zone, many potential sources of anisotropy may contribute to the observed signal, but if we have a good understanding of LPO fabrics (and the conditions under which they occur), then we can use anisotropy observations to infer the pattern of deformation and flow in the mantle. In this study we explore how the mantle above the Peruvian flat slab has responded to the evolution of flat subduction. We present observations of seismic anisotropy from local *S* splitting measurements to infer mantle deformation associated with the spatiotemporal progression of slab flattening.
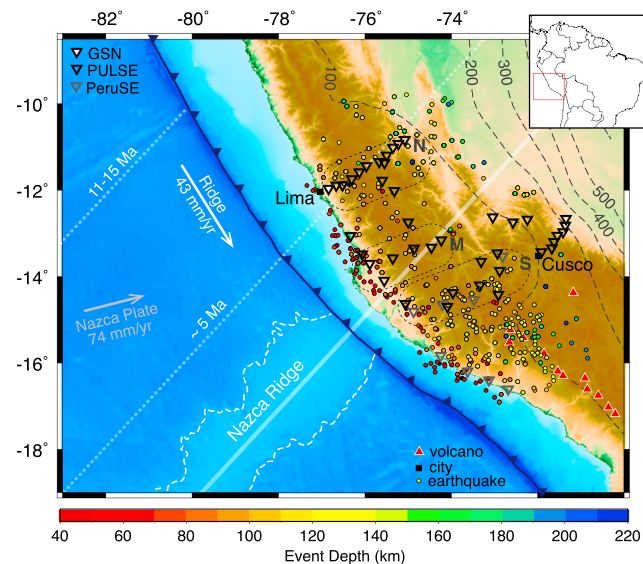
Figure 1. Tectonic setting and station locations. Slab contours (dashed dark grey lines) are from the Slab 1.0 model (unit: km) [*Hayes et al.*, 2012]. Map shows distribution of seismicity (small circles colored by depth) and stations (triangles color coded by seismic network) used in this study. The northern, middle, and southern PULSE lines are enclosed by the thin dashed circles and labeled with N, M, and S, respectively. Thick white line shows continuation of the subducted Nazca Ridge. Dotted white lines show estimated position of the ridge in the past [*Hampel*, 2002]. Grey arrow represents the absolute plate motion of the Nazca plate from HS3-NUVEL1A [*Gripp and Gordon*, 2002]. Volcano locations (red triangles) are from *Siebert and Simkin* [2002].

2. Tectonic Evolution of the Peruvian Flat Slab

The subduction zone beneath Peru in South America represents one of the best localities available to study the dynamics of flat slab systems. Extending over 1500 km along strike (3°S to 15°S), the Peruvian flat slab segment is by far the most extensive present-day region of flat subduction in the world (Figure 1) [*Cahill and Isacks*, 1992; *Hayes et al.*, 2012]. The slab subducts normally at the trench to a depth of ~100 km and then travels horizontally for several hundred kilometers before steepening again to the east [*Cahill and Isacks*, 1992; *Ma and Clayton*, 2014; *Phillips and Clayton*, 2014]. The region is characterized by a distinct lack of contemporary volcanism and low heat flow (~20 mW/m^2) [*Henry and Pollack*, 1988], in contrast to the normally dipping (~30°) regions to the north and south.

A distinguishing characteristic of the Peruvian flat slab segment is its association with the subduction of the Nazca Ridge at 14–17°S on the Peru-Chile trench (Figure 1). The Nazca Ridge is over 1000 km long and 200 km wide and sits at an elevation of 1500 m above the surrounding seafloor [*Hampel*, 2002]. The ridge is compensated by an abnormally thick oceanic crust, estimated from seismic and gravity data to be about 17–18 km thick [*Couch and Whitsett*, 1981; *Woods and Okal*, 1994; *Hampel*, 2004]. The Nazca Ridge first intersected the Peru-Chile trench at ~9–11°S approximately 11–15 million years ago and since then has been sweeping south across southern Peru due to its oblique geometry [*Hampel*, 2002; *Rosenbaum et al.*, 2005]. At its current position, the subduction of buoyant Nazca Ridge material has been associated with several distinctive characteristics of the overriding plate, including enhanced tectonic erosion at the margin, a westward shift of the coastline, and uplift of the Fitzcarrald Arch in the Amazonian foreland [*Hampel*, 2004; *Espurt et al.*, 2007].

In the Peruvian flat slab region the overriding continental crust has been estimated to be approximately 50–70 km thick beneath the sub-Andes [*Feng et al.*, 2007; *Lloyd et al.*, 2010; *Phillips and Clayton*, 2014], thinning toward the east to 35–44 km beneath the foreland basins [*James and Snoke*, 1994]. If the top of the flat slab is at ~100 km depth [*Cahill and Isacks*, 1992], then this leaves ~30–50 km of space for mantle material between the slab interface and the overriding crust. Where the Nazca Ridge is subducting the slab is even shallower [*Kumar et al.*, 2013], and receiver function analysis suggests that the subducted ridge and overriding continental crust are essentially in direct contact, with little, if any, mantle sandwiched in between [*Bishop et al.*, 2013]. The constriction of the mantle wedge between the flat slab and continental crust most certainly inhibits typical asthenospheric corner flow and therefore provides the most likely explanation for the lack of volcanism above flat slabs [*Barazangi and Isacks*, 1976].

Little is known about the properties of the thin mantle wedge that does remain above flat slabs after typical corner flow has ceased. The proximity of the cold, subducting oceanic lithosphere likely reduces the temperature, increasing the viscosity and making the mantle harder to deform [e.g., *Wagner et al.*, 2006]. The properties of the supraslab mantle could be altered by the addition of volatiles or compositional changes such as orthopyroxene enrichment [*Wagner et al.*, 2008], but little is known about the details of these processes or how volatiles cycle through the flat slab system. The physical properties of the mantle above flat

slabs have major implications for the degree of coupling and stress transfer between the flat slab and the overlying continent, and understanding them is therefore key to understanding the surface expressions of flat subduction. The spatiotemporal progression of the Nazca Ridge southward through the Peruvian flat slab system makes this locale a particularly compelling region in which to study of properties of the supraslab mantle.

3. Local *S* Wave Splitting Analysis: Data and Methods

Seismic anisotropy describes the directional dependence of seismic wave speed and is an indicator for past and/or ongoing deformation in the Earth's interior. When a shear wave passes through an anisotropic medium, it will be polarized into two quasi-*S* waves, one corresponding to a fast direction (φ) and one to a slow direction, in a phenomenon known as shear wave splitting. The fast and slow phases accumulate a delay time (δt) between them that depends upon the strength of the anisotropy and the path length through the anisotropic material.

In this study we analyzed shear wave splitting at 49 broadband stations located over the southern part of the Peruvian flat slab region (Figure 1). Forty of these stations were deployed as the PULSE (PerU Lithosphere and Slab Experiment) array, which operated from October 2010 until June 2013. This array was deployed as three transects roughly perpendicular to the trench (with additional stations between) that we refer to as the northern, middle, and southern lines (see Figure 1). The middle line lies above the projection of the subducting Nazca Ridge. We also include data from eight stations of the PeruSE network (Peru Subduction Experiment) [*PeruSE*, 2013], with data available from November 2010 until April 2013. Over the same time period, we also analyzed data from one permanent Global Seismographic Network (GSN) station (NNA) located within the region.

For each station we examined local *S* events occurring within the Peruvian subduction zone. Event locations and origin times were obtained from a regional earthquake catalog compiled by the Instituto Geofísico del Perú using data from the Peruvian national seismic network, as this provides by far the densest coverage in our study region. It should be noted, however, that this catalog has not yet been hypocenter relocated, so the depths are approximate, with average depth uncertainties estimated at ±10 km. The event locations are typically deeper than the Slab 1.0 contours [*Hayes et al.*, 2012] (Figures 1 and 2), as well as the smaller (relocated) catalog of *Kumar et al.* [2013] by ~15 km on average (see Figure S5 in the supporting information), but sometimes up to 40 km deeper especially for the deepest events. We considered events of magnitude 4.0 and above and depths greater than 40 km and limited our analysis to raypaths that arrive with incidence angles under 35° in order to avoid phase conversions at the surface [e.g., *Evans*, 1984]. This provided a useful event list of 370 earthquakes for which we could investigate shear wave splitting (Figure 1).

Shear wave splitting analyses for every eligible event-station pair were carried out using the SplitLab software package [*Wüstefeld et al.*, 2008]. We report splitting parameters (φ and δt) obtained using the rotation correlation (RC) method [*Bowman and Ando*, 1987], but we also estimated splitting parameters using the eigenvalue (EV) method [*Silver and Chan*, 1991] to compare and assess reliability. We applied a variable band-pass filter to all waveforms to improve the signal-to-noise ratio. The low-frequency cutoff was typically 0.5 Hz (min: 0.2 Hz, max: 0.8 Hz) and the high-frequency cutoff 1.5 Hz (min: 1.0 Hz, max: 2.0 Hz). All measurements were quality assessed based upon a visual inspection of the particle motions (elliptical initially and linearized once corrected) and the corrected waveforms (similar pulse shapes in the fast and slow components). We retained high-quality measurements with 2σ errors of less than 25° in φ and less than 0.15 s in δt. Between the RC and EV methods, we allowed the splitting parameters to differ by up to 25° in φ and 0.1 s in δt. Null measurements (i.e., shear wave arrivals that have not undergone splitting) were identified based upon a clearly visible *S* pulse, with high signal-to-noise and linear initial particle motion.

4. Results

Our analysis resulted in 380 high-quality splitting measurements and 70 null measurements at 49 stations across southern Peru. Delay times are typically moderate (90% less than 0.5 s), most likely due to the high-frequency content of the local *S* phases (Figure S1) and the relatively short raypaths. The results are shown in map view in Figure 2, sorted by event depth into 20 km bins to illustrate the spatial and depth variability.
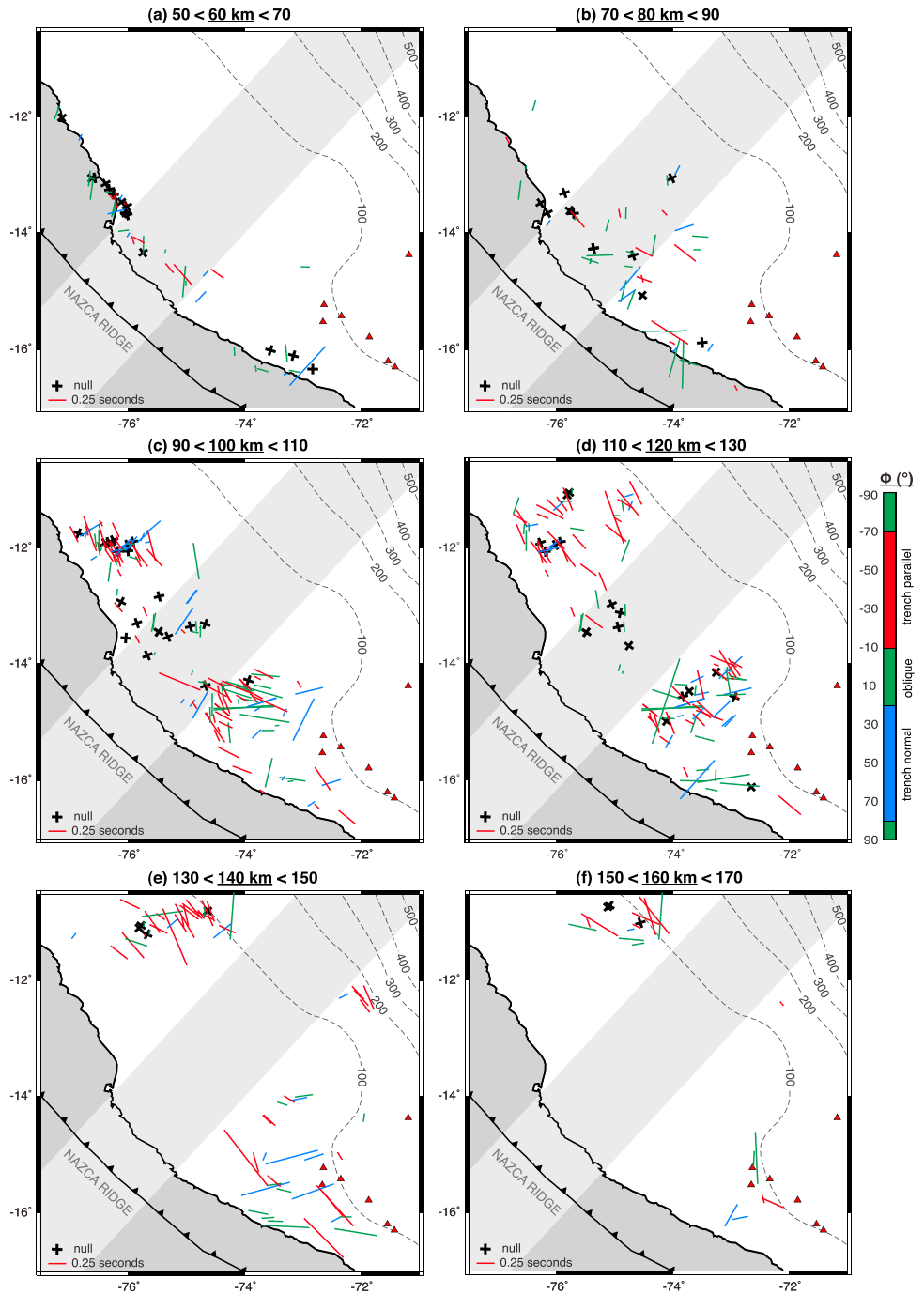
Figure 2. (a–f) Local S splitting results separated by event depth ranges. Each splitting measurement is represented by a bar, oriented and colored by ϕ (see color scale on the right), and scaled in length by δt (0.25 s example shown in the legend). Null measurements are represented by small black crosses, which are aligned according to the possible fast/slow directions derived from S wave polarization measurements. All measurements are plotted at the event location (i.e., at their source). Light grey band across the region highlights the estimated area of the subducting Nazca Ridge. Slab contours and volcano locations are the same as in Figure 1.

At the shallowest event depths (<70 km: Figure 2a), earthquakes are located mostly near the trench, and our measurements therefore only sample the continental crust. Our shallowest splitting measurements are variable, with small delay times (86% of delay times ≤0.25 s, mean: 0.18 s), and there are a relatively high proportion of nulls (37%, compared to 18% for the whole data set). At deeper event depths (Figures 2c–2f),

the splitting measurements start to show coherent spatial patterns. To the north of the ridge (along the PULSE northern line), the fast directions show a predominately NW-SE orientation (red bars in Figures 2c–2f), although there is some scatter in the results. This orientation is approximately parallel to both the trench strike and the trend of high topography (see histogram in Figure S2a). Many of the null observations are also in agreement with this orientation (Figure S2a), exhibiting polarization directions that are nearly parallel to the observed fast splitting directions. Average delay times in the north for events deeper than 90 km are moderate, with a mean of 0.27 s, and show a tendency to increase with event depth (Figure S3a).

To the south of the ridge (along the PULSE southern line), where the slab is flat but is adjacent to the transition to steeper subduction, we obtained a large number of splitting results for events deeper than 90 km (Figures 2c–2e). These are similar to the north in terms of magnitude (mean δt: 0.29 s) but not in fast directions; measured φ values are scattered, with no clear dominant orientation (Figures 2c–2f and S2c). Additionally, delay times in the south do not show a clear trend with event depth (Figure S3c). Over the Nazca Ridge itself, where the middle line of PULSE stations are situated, the splitting pattern is quite different. Here observed delay times are small (mean δt: 0.16 s) in comparison to the north and south (Figures S2d–S2f), and over 40% of the measurements are null observations (Figures 2c, 2d, and S2b) that cover a range of initial polarization directions.

5. Discussion

The results presented here provide the first observations that directly constrain seismic anisotropy above the Peruvian flat slab. We have previously studied shear wave splitting from teleseismic phases at station NNA, located at the western end of the PULSE northern line, and modeled the results with multiple layers of anisotropy [*Eakin and Long*, 2013]. The preferred model invoked a two-layer anisotropic structure beneath NNA, with the upper layer (inferred to be above the slab) oriented generally WNW-ESE (i.e., trench oblique to trench parallel). The NW-SE trending fast directions from local *S* measurements reported in this study along the PULSE northern line (i.e., north of the ridge) are in rough approximation with this modeled upper layer. The delay times, however, are much larger in the model (~ 2.5 s) compared to our results (typically <0.5 s), which may be due in part to the differing frequency content (and therefore Fresnel zone size) between local *S* (~ 1.2 Hz) and teleseismic (0.05–0.5 Hz) phases used by each study. Strong frequency-dependent delay times, with lower frequencies yielding longer delays, have already been documented beneath NNA [*Eakin and Long*, 2013].

For comparison, *MacDougall et al.* [2012] studied shear wave splitting from local *S* events above the Pampean flat slab and found delay times similar in magnitude to ours (~0.26 s), as well as variable fast directions that resemble our observations south of the ridge. The source of anisotropy there was inferred to reside mainly in the mantle wedge, resulting from two-dimensional corner flow that is partially deflected by pressure gradients due to the decrease in slab dip.

The observed pattern of shear wave splitting above the Peruvian flat slab is consistent with suggestions made by earlier work [*Eakin and Long*, 2013], but the interpretation of this pattern involves constraining the precise location of anisotropy within the subduction system. There are three reasonable possibilities: the continental crust, the upper portion of the slab itself, or the mantle material in between. It seems unlikely that the crust makes the primary contribution to the majority of our splitting observations. For raypaths that mainly sample the crust (Figure 2a), we observe small delay times (median δt: 0.16 s) and a large number of null measurements. A primary contribution from the continental crust is also inconsistent with the increasing delay times with event depth observed in the north (Figure S3a) and a lack of correlation between delay time and incidence angle (Figure S4). In addition, crustal stress orientations over southern Peru are mostly SE-NW or E-W [*Heidbach et al.*, 2008]; a stress-aligned fracture induced model for crustal anisotropy [e.g., *Crampin*, 1994] would predict trench-normal fast directions, inconsistent with observations. We therefore infer that crustal anisotropy is likely present but variable and weak and might contribute to the observed scatter in the data, imprinting over a deeper but more dominant anisotropic signal.

A contribution from the shallow part of the slab itself (e.g., from combined shape-preferred orientation (SPO) and LPO of hydrated faults in the slab crust) [*Faccenda et al.*, 2008; *Healy et al.*, 2009] is possible and cannot be ruled out. Many of the earthquakes used in this study likely originate near the top of the slab, and so the portions of the raypaths that sample the slab are likely to be generally short. There are, however, some deeper events in the catalog (Figures 2d–2f), whose depth estimates are questionable (Figure S5), but if

located correctly would have significantly longer paths through the slab, and potentially a greater contribution from slab anisotropy. While there is evidence for substantial anisotropy within the subducting Nazca slab [*Eakin and Long*, 2013], it is not clear that a primary contribution from slab anisotropy could explain the spatial variations in splitting behavior documented in this study.

We suggest, instead, that the most likely dominant source of anisotropy sampled by our data set is in the mantle material between the slab interface and the base of the continental crust. This inference is supported by the spatial variations in splitting we observe along strike. Specifically, we observe considerable splitting to the north and south of the Nazca Ridge but very little over the ridge itself, where the slab is shallowest and the mantle "wedge" material is at its thinnest (Figure 2). If the mantle sandwiched between the slab and the continental crust is indeed anisotropic, then the anisotropy is most likely generated by the LPO of anisotropic minerals. For example, one possibility is that anisotropy in the mantle is due to the LPO of hydrous phases, such as serpentine, which form where the mantle is hydrated by water released from the subducting slab below [e.g., *Hilairet and Reynard*, 2009]. During simple shear deformation of serpentine minerals, the *c* axis (slow axis) tends to align perpendicular to the shear plane [*Katayama et al.*, 2009; *Jung*, 2011]. The other remaining two axes align within the shear plane and exhibit very similar *S* wave velocities. For the simple case where the shear plane is aligned with the flat slab surface, (nearly) vertically incident shear waves should not sense much of a velocity difference or therefore undergo much splitting. Serpentinite LPO therefore seems to be a less likely explanation for our measurements, although we cannot rule out more complicated deformation geometries or a contribution from other hydrous phases.

The most common scenario for upper mantle anisotropy is the LPO of olivine, and it is this mechanism that we favor as the most likely explanation for our observations. Deformation under typical mantle conditions produces A-, C-, or E-type fabrics; in these cases, the fast splitting direction tends to correspond to the shear direction [e.g., *Karato et al.*, 2008]. Under certain conditions, however, B-type olivine fabric is expected [*Jung and Karato*, 2001; *Jung et al.*, 2006], whereby the fast axis will align perpendicular to the shear direction. Geodynamical modeling suggests that B-type fabric may exist in the fore-arc mantle wedge where low temperature, high stress, and water-rich conditions prevail [*Kneller et al.*, 2005, 2007]. Such conditions may also exist in the mantle sandwiched between the Peruvian flat slab and continental crust, so B-type fabric is a possibility. In most cases where B-type fabric is inferred, however, a transition in φ is observed from the fore arc to the back arc, corresponding to the change in fabric type [e.g., *Nakajima and Hasegawa*, 2004; *Long and van der Hilst*, 2006]. We might also expect to see such a transition for the Peruvian supraslab mantle due to variations in water content and/or stress across the 500 km wide flat slab region. Evidence for spatial gradients in hydration above a flat slab, which could induce a fabric transition, has been previously documented in the Pampean region [e.g., *Porter et al.*, 2012], which is much less spatially extensive than the flat slab beneath Peru. The consistency of our observations of trench-parallel φ north of the ridge, even for events occurring over 250 km away from the trench, argues against such a fabric transition. It can be deduced, therefore, that either the conditions required for B-type fabric persist across the entire flat slab segment or the presence of other olivine fabrics (A, C, or E type) is more likely.

The magnitudes of our observed delay times are also consistent with an olivine LPO scenario. To the north and south of the ridge, we observed mean delay times of 0.27 s and 0.29 s, respectively. Following *Silver and Chan* [1988], assuming an isotropic shear wave velocity of 4.6 km/s and a path length of 30 km through the mantle [*Bishop et al.*, 2013; *Phillips and Clayton*, 2014], our observed delay times suggest that the strength of anisotropy is ~4%. If we allow for a small (up to ~0.15 s) contribution to splitting from the continental crust or the slab, our estimate for the anisotropy strength would be slightly lower. Either way, around 3–4% anisotropy is consistent with the expectation for deformed olivine-bearing peridotite [*Christensen and Lundquist*, 1982].

Based on the above arguments, our preferred interpretation of local *S* splitting beneath the Peruvian flat slab is that it results primarily from A-, C-, or E-type olivine LPO in the mantle material sandwiched between the slab and the overriding continental crust, generated either by present-day or past deformational processes. Given the spatial variations in splitting patterns documented here and their relationships with the ongoing southward progression of the Nazca Ridge, we suggest the following scenario (Figure 3). To the north of the ridge, we propose that the mantle wedge deformed coherently via trench-parallel shearing during (or shortly
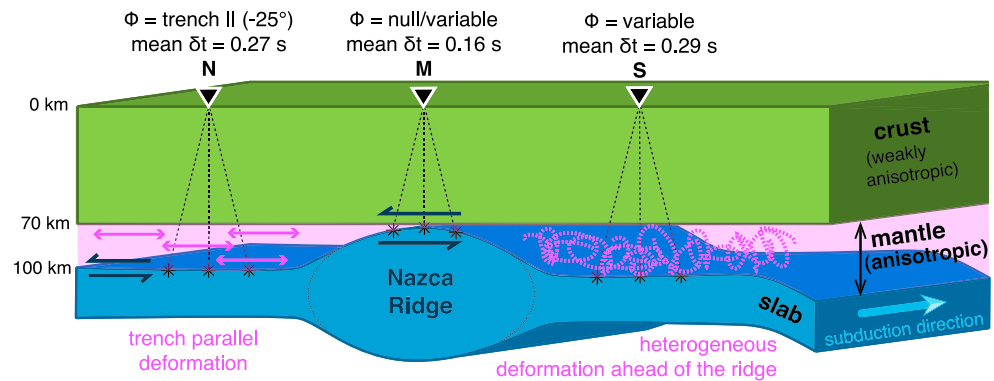
Figure 3. Schematic cross section through the Peruvian flat slab region (parallel to the trench) summarizing the shear wave splitting results and illustrating our preferred deformation scenario. The main source of anisotropy appears to be located in the 30 km thick wedge of mantle material between the flat slab and the continental crust. This layer is thinnest above the ridge, where the weakest splitting is seen. To the north and south of the ridge, the different anisotropic patterns reflect different deformational regimes controlled by the southward migration of the Nazca Ridge, with trench-parallel shearing in the north and complex, heterogeneous deformation in the south. N, M, and S labeled above the station symbols (black triangles) are the same as for Figure 1.

after) the passage of the ridge and that the fast directions we observe in the remnant mantle wedge reflect the imprint of this deformation. Our observations do not constrain whether this deformation signature reflects the influx of new asthenospheric material behind the ridge or trench-parallel shearing of the original mantle lithosphere as the ridge passed underneath. Given that the total volume of ridge material that has subducted is increasing over time, it is possible that in the past the Nazca slab was not as buoyant or as shallow as it is today, and that a layer of mantle lithosphere could still remain in place beneath the overriding plate to the north of the present-day ridge location. To the south of the ridge, where the ridge has not yet passed, the splitting pattern we observe (with variable φ and delay times comparable to the north) suggests a deformation pattern that is spatially heterogeneous and incoherent. We hypothesize that the southward progression of the ridge as it pushes its way through the mantle may result in strong but heterogeneous deformation of the mantle wedge directly in front of the ridge.

There are alternatives to our preferred scenario that may explain some aspects of the observed splitting patterns. For example, trench-parallel fast directions in the north could be explained by the trench-perpendicular compression or shortening of the mantle lithosphere; in conjunction with the trench-parallel migration of the ridge, this could result in considerable extension (i.e., flow) of the mantle along strike. We also cannot rule out the presence of B-type olivine fabric in the north, which might suggest a different deformation geometry as the ridge passed by (i.e., trench-normal shear instead of trench parallel), although this is not incompatible with our general scenario. The variable splitting pattern in the south of our study area, which we attribute to heterogeneous deformation induced by the southward progression of the ridge, could also be potentially explained by multiple layers of anisotropy or by the nearby transition from flat to normal subduction. The changing slab morphology could be causing complex flow in the mantle wedge, introducing a dipping component of anisotropy, or causing variable states of stress and hydration in the mantle that lead to a mix of olivine fabrics (potentially including B type).

6. Conclusion

We propose a scenario for southern Peru in which the deformation of the supraslab mantle is controlled by the migration of the Nazca Ridge. This implies that the mantle is being deformed, at least in part, by the subducting plate and that there is some degree of coupling and upward transfer of stress between the flat slab and the upper plate. There is, however, little evidence preserved in the anisotropic fabric for widespread basal shear from the flat slab in the downdip direction along the base of the upper plate, as might have been expected. Given the estimated strength of anisotropy, it is also unlikely that the mantle is widely serpentinized or hydrated above the flat slab, which could have resulted in a weaker mantle rheology. Our measurements cannot, however, rule out the presence of a thin layer (on the order of several kilometers) or localized pockets of serpentinized mantle.

References

Barazangi, M., and B. L. Isacks (1976), Spatial distribution of earthquakes and subduction of the Nazca plate beneath South America, *Geology*, *4*(11), 686–692.

Bird, P. (1988), Formation of the Rocky Mountains, western United States—A continuum computer model, *Science*, *239*, 1501–1507.

Bishop, B., S. Beck, G. Zandt, A. Kumar, L. Wagner, M. Long, and H. Tavera (2013), Receiver function study of the Peruvian flat-slab region: Initial results from PULSE, AGU Fall Meeting 2013, San Francisco.

Bowman, J. R., and M. Ando (1987), Shear-wave splitting in the upper-mantle wedge above the Tonga subduction zone, *Geophys. J. Int.*, *88*(1), 25–41, doi:10.1111/j.1365-246X.1987.tb01367.x.

Cahill, T., and B. L. Isacks (1992), Seismicity and shape of the subducted Nazca Plate, *J. Geophys. Res.*, *97*(B12), 17,503–17,529, doi:10.1029/92JB00493.

Christensen, N. I., and S. M. Lundquist (1982), Pyroxene orientation within the upper mantle, *Geol. Soc. Am. Bull.*, *93*(4), 279–288, doi:10.1130/0016-7606(1982)93.

Coney, P., and S. Reynolds (1977), Cordilleran Benioff zones, *Nature*, *270*, 403–406.

Couch, R., and R. M. Whitsett (1981), Structures of the Nazca Ridge and the continental shelf and slope of southern Peru, in *Nazca Plate: Crustal Formation and Andean Convergence*, edited by L. D. Kulm et al., *Mem. Geol. Soc. Am.*, *154*, 569–586.

Crampin, S. (1994), The fracture criticality of crustal rocks, *J. Geophys. Res.*, *118*, 428–438.

Dickinson, W., and W. Snyder (1978), Plate tectonics of the Laramide orogeny, *Geol. Soc. Am. Mem.*, *151*, 355–366.

Eakin, C., and M. Long (2013), Complex anisotropy beneath the Peruvian flat slab from frequency-dependent, multiple-phase shear wave splitting analysis, *J. Geophys. Res. Solid Earth*, *118*, 4794–4813, doi:10.1002/jgrb.50349.

Espurt, N., P. Baby, S. Brusset, M. Roddaz, W. Hermoza, V. Regard, P.-O. Antoine, R. Salas-Gismondi, and R. Bolaños (2007), How does the Nazca Ridge subduction influence the modern Amazonian foreland basin?, *Geology*, *35*(6), 515, doi:10.1130/G23237A.1.

Evans, R. (1984), Effects of the free surface on shear wave trains, *Geophys. J. Int.*, *76*(1), 165–172.

Faccenda, M., L. Burlini, T. V. Gerya, and D. Mainprice (2008), Fault-induced seismic anisotropy by hydration in subducting oceanic plates, *Nature*, *455*(7216), 1097–1100, doi:10.1038/nature07376.

Feng, M., S. van der Lee, and M. Assumpção (2007), Upper mantle structure of South America from joint inversion of waveforms and fundamental mode group velocities of Rayleigh waves, *J. Geophys. Res.*, *112*, B04312, doi:10.1029/2006JB004449.

Gripp, A. E., and R. G. Gordon (2002), Young tracks of hotspots and current plate velocities, *Geophys. J. Int.*, *150*(2), 321–361, doi:10.1046/j.1365-246X.2002.01627.x.

Hampel, A. (2002), The migration history of the Nazca Ridge along the Peruvian active margin: A re-evaluation, *Earth Planet. Sci. Lett.*, *203*, 665–679.

Hampel, A. (2004), Ridge subduction at an erosive margin: The collision zone of the Nazca Ridge in southern Peru, *J. Geophys. Res.*, *109*, B02101, doi:10.1029/2003JB002593.

Hayes, G., D. Wald, and R. Johnson (2012), Slab1. 0: A three-dimensional model of global subduction zone geometries, *J. Geophys. Res.*, *117*, B01302, doi:10.1029/2011JB008524.

Healy, D., S. M. Reddy, N. E. Timms, E. M. Gray, and A. V. Brovarone (2009), Trench-parallel fast axes of seismic anisotropy due to fluid-filled cracks in subducting slabs, *Earth Planet. Sci. Lett.*, *283*(1–4), 75–86, doi:10.1016/j.epsl.2009.03.037.

Heidbach, O., M. Tingay, A. Barth, J. Reinecker, D. Kurfeß, and B. Müller (2008), The world stress map database release 2008, doi:10.1594/GFZ.WSM. Rel2008.

Henry, S. G., and H. N. Pollack (1988), Terrestrial heat flow above the Andean subduction zone in Bolivia and Peru, *J. Geophys. Res.*, *93*(B12), 15,153–15,162, doi:10.1029/JB093iB12p15153.

Hilairet, N., and B. Reynard (2009), Stability and dynamics of serpentinite layer in subduction zone, *Tectonophysics*, *465*(1–4), 24–29, doi:10.1016/j.tecto.2008.10.005.

Humphreys, E. (2009), Relation of flat subduction to magmatism and deformation in the western United States, in *Backbone of the Americas: Shallow Subduction, Plateau Uplift, and Ridge and Terrane Collision*, edited by S. M. Kay, V. A. Ramos, and W. R. Dickinson, *Geol. Soc. Am. Mem.*, *204*, 85–98, doi:10.1130/2009.1204(04).

James, D., and J. Snoke (1994), Structure and tectonics in the region of flat subduction beneath central Peru: Crust and uppermost mantle, *J. Geophys. Res.*, *99*(B4), 6899–6912.

Jung, H. (2011), Seismic anisotropy produced by serpentine in mantle wedge, *Earth Planet. Sci. Lett.*, *307*(3–4), 535–543, doi:10.1016/j.epsl.2011.05.041.

Jung, H., and S. Karato (2001), Water-induced fabric transitions in olivine, *Science*, *293*(5534), 1460–3, doi:10.1126/science.1062235.

Jung, H., I. Katayama, Z. Jiang, T. Hiraga, and S. Karato (2006), Effect of water and stress on the lattice-preferred orientation of olivine, *Tectonophysics*, *421*(1–2), 1–22, doi:10.1016/j.tecto.2006.02.011.

Karato, S., H. Jung, I. Katayama, and P. Skemer (2008), Geodynamic significance of seismic anisotropy of the upper mantle: New insights from laboratory studies, *Annu. Rev. Earth Planet. Sci.*, *36*(1), 59–95, doi:10.1146/annurev.earth.36.031207.124120.

Katayama, I., K. Hirauchi, K. Michibayashi, and J. Ando (2009), Trench-parallel anisotropy produced by serpentine deformation in the hydrated mantle wedge, *Nature*, *461*(7267), 1114–7, doi:10.1038/nature08513.

Kneller, E. A., P. E. van Keken, S. Karato, and J. Park (2005), B-type olivine fabric in the mantle wedge: Insights from high-resolution non-Newtonian subduction zone models, *Earth Planet. Sci. Lett.*, *237*(3–4), 781–797, doi:10.1016/j.epsl.2005.06.049.

Kneller, E. A., P. E. van Keken, I. Katayama, and S. Karato (2007), Stress, strain, and B-type olivine fabric in the fore-arc mantle: Sensitivity tests using high-resolution steady-state subduction zone models, *J. Geophys. Res.*, *112*, B04406, doi:10.1029/2006JB004544.

Kumar, A., L. Wagner, S. Beck, B. Young, G. Zandt, M. Long, H. Tavera, and E. Minaya (2013), Determination of Nazca slab geometry and state of stress beneath the southern Peru and northern Bolivia, AGU Fall Meeting 2013, San Francisco, Calif.

Lloyd, S., S. van der Lee, G. S. França, M. Assumpção, and M. Feng (2010), Moho map of South America from receiver functions and surface waves, *J. Geophys. Res.*, *115*, B11315, doi:10.1029/2009JB006829.

Long, M. D., and R. D. van der Hilst (2006), Shear wave splitting from local events beneath the Ryukyu arc: Trench-parallel anisotropy in the mantle wedge, *Phys. Earth Planet. Inter.*, *155*(3), 300–312.

Long, M. D., and T. W. Becker (2010), Mantle dynamics and seismic anisotropy, *Earth Planet. Sci. Lett.*, *297*, 341–354.

Ma, Y., and R. W. Clayton (2014), The crust and uppermost mantle structure of Southern Peru from ambient noise and earthquake surface wave analysis, *Earth Planet. Sci. Lett.*, *395*, 61–70.

MacDougall, J. G., K. M. Fischer, and M. L. Anderson (2012), Seismic anisotropy above and below the subducting Nazca lithosphere in southern South America, *J. Geophys. Res.*, *117*, B12306, doi:10.1029/2012JB009538.

Nakajima, J., and A. Hasegawa (2004), Shear-wave polarization anisotropy and subduction-induced flow in the mantle wedge of northeastern Japan, *Earth Planet. Sci. Lett.*, *225*(3), 365–377.

PeruSE (2013), Peru subduction experiment, *Caltech*, Dataset, doi:10.7909/C3H41PBZ.

Phillips, K., and R. W. Clayton (2014), Structure of the subduction transition region from seismic array data in southern Peru, *Geophys. J. Int.*, *196*, 1889–1905, doi:10.1093/gji/ggt504.

Porter, R., H. Gilbert, G. Zandt, S. Beck, L. Warren, J. Calkins, P. Alvarado, and M. Anderson (2012), Shear wave velocities in the Pampean flat slab region from Rayleigh wave tomography: Implications for slab and upper mantle hydration, *J. Geophys. Res.*, *117*, B11301, doi:10.1029/2012JB009350.

Ramos, V. A., and A. Folguera (2009), Andean flat-slab subduction through time, *Geol. Soc. London, Spec. Publ.*, *327*(1), 31–54, doi:10.1144/SP327.3.

Rosenbaum, G., D. Giles, M. Saxon, P. G. Betts, R. F. Weinberg, and C. Duboz (2005), Subduction of the Nazca Ridge and the Inca Plateau: Insights into the formation of ore deposits in Peru, *Earth Planet. Sci. Lett.*, *239*(1–2), 18–32, doi:10.1016/j.epsl.2005.08.003.

Siebert, L., and T. Simkin (2002), Volcanoes of the world: An illustrated catalog of Holocene volcanoes and their eruptions. Global Volcanism Program Digital Information Series, GVP-3, Smithsonian Institution, Washington, D. C. [Available at http://www.volcano.si.edu/world/.]

Silver, P., and W. Chan (1988), Implications for continental structure and evolution from seismic anisotropy, *Nature*, *335*, 34–39.

Silver, P., and W. Chan (1991), Shear wave splitting and subcontinental mantle deformation, *J. Geophys. Res.*, *96*(B10), 16,429–16,454.

Wagner, L. S., S. L. Beck, G. Zandt, and M. Ducea (2006), Depleted lithosphere, cold, trapped asthenosphere, and frozen melt puddles above the flat slab in central Chile and Argentina, *Earth Planet. Sci. Lett.*, *245*, 289–301.

Wagner, L. S., M. L. Anderson, J. Jackson, S. L. Beck, and G. Zandt (2008), Seismic evidence for orthopyroxene enrichment in the continental lithosphere, *Geology*, *36*, 935–938.

Woods, M. T., and E. a. Okal (1994), The structure of the Nazca Ridge and Sala Y Gomez seamount chain from the dispersion of Rayleigh waves, *Geophys. J. Int.*, *117*(1), 205–222, doi:10.1111/j.1365-246X.1994.tb03313.x.

Wüstefeld, A., G. Bokelmann, C. Zaroli, and G. Barruol (2008), SplitLab: A shear-wave splitting environment in Matlab, *Comput. Geosci.*, *34*(5), 515–528, doi:10.1016/j.cageo.2007.08.002.